This full text paper was peer reviewed at the direction of IEEE Communications Society subject matter experts for publication in the IEEE ICC 2011 proceedings

RF Emitter Location Using A Network of Small Unmanned Aerial Vehicles (SUAVs)

Jing Liang and Qilian Liang, *Senior Member, IEEE*
Department of Electrical Engineering
University of Texas at Arlington
Arlington, TX 76019-0016 USA
E-mail: jliang@wcn.uta.edu, liang@uta.edu

***Abstract*—In this paper, we design a network of small unmanned aerial vehicles (SUAVs) for passive location of RF emitters. Each small UAV is equipped with multiple electronic surveillance (ES) sensors to provide local mean distance estimation based on the received signal strength indicator (RSSI). Fusion center will determine the location of the target via UAV triangulation. Different with the previous existing studies, our method is on a basis of an empirical path loss and log-normal shadowing model, from a wireless communication and signal processing vision to offer an effective solution. The performance degradation between UAVs and fusion center is taken into consideration rather than assuming lossless communication. We analyze the geolocation error and the error probability of distance based on the proposed system. The result shows that this approach provides robust performance for high frequency RF emitters.**

I. Introduction and Motivation

Currently, there is a developing trend to use passive location approach for RF emitters. Unmanned aerial vehicle (UAVs) is of most interest owing to better grazing angles closer to the target than large dedicated manned surveillance platforms [1]. In addition, UAVs are capable of continuous 24-hour surveillance coverage. To this date, the concept of UAV is not only limited to an unpiloted aircraft, but unmanned aerial systems (UAS) including ground stations and other elements as well.

Small unmanned aerial systems (SUAS) are rapidly gaining popularity due to the miniaturization of RF components and processors. In particular, given the cutting-edge technology in modern remote sensing (RS), SUAS can be equipped with electronic surveillance (ES) sensors in place of bulky active radars, which result in smaller, lighter and lower-cost counterparts. These types of SUAS are generally classified as having a wing-span of less than 4 meters [2] and a gross vehicle weight less than 15 pounds [3]. A number of UAV manufacturers have developed low-cost TDMA data links that support the cooperative team work of multiple UAVs, which provides higher mobility, survivability and closer proximity to the targeting emitters.

In the present work, [3] and [4] are based on a team of UAVs working cooperatively with on-board camera systems. The location of an object is determined by the fusion of camera images. However, the visual feature can become vulnerable in the following cases: 1)when telemetry and image streams are not synchronized, the target coordinates read by UAV can be particularly misleading; 2)when weather is severe and visibility is low, the image based geolocation may not provide day-or-night, all-weather surveillance; 3)target is well protected and hidden, such as deeply beneath the foliage.

Besides visual feature, the time difference of arrival (TDOA) technique has been adopted in the current work [5]-[9]. In these investigations, a network of at least three UAVs has been employed with on-board ES sensors, a global positioning system (GPS) receiver and a precision clock. When the target is detected by the sensor, the time of arrival would be transmitted to a fusion center, which would finally estimate the emitter location based on their TDOA. Also, Kalman filters is used to track the object. However, TDOA, like other methods including Angle of Arrival (AOA), Frequency of Arrival (FOA), Frequency Difference of Arrival (FDOA) and Phase Difference of Arrival (PDOA) etc., is well known for difficult synchronization issues, such as fine synchronization for location algorithms and coarse synchronization for the coordinating data collected within the area of interest at a common time.

In this paper, we apply netcentric SUAS with on-board multiple ES sensors for RF emitter location. Different from previous work described above, our work describes about a complete system design and analyze the performance in detail. Our method is on a basis of an empirical pass loss and log-normal shadowing model, which has been adopted for reliable high-speed wireless communications for moving users in dynamic environment, but has never been used in the SUAS before, to the best of our knowledge. Also, the performance of multiple ES sensors will be considered for the system as a whole. In addition, we will provide a confidence assessment through error bounding, which has not been seen in the existing approaches.

The rest of paper is organized as follows. Section II presents the system design based on path loss and log-normal shadowing model. Section III analyzes performance of netcentric decision. Section IV presents simulation results and illustrate the characteristics of the approach. Finally, section V draws the conclusion.

978-1-61284-233-2/11/$26.00 ©2011 IEEE

II. Path Loss and Log-normal shadowing Approach

In our work, we assume the SUAS is composed of $R(R \geq 3)$ small UAVs. Each UAV is equipped with $N(N \geq 1)$ ES sensors, whose task is to provide received signal strength indicator (RSSI) of RF emitters. A processor is also on-board to compute the current distance from the RF emitter to the sensors based on RSSI. Notice that even though the computation can be achieved in a very fast time on a basis of detected RSSI, estimated distance poses drifts from the real distance due to the relative motion between the UAV and the RF emitter as well as wind gusts during the moment of computation. Thus multiple sensors are employed to provide the receiver diversity. Later we will show that multiple sensors help reduce the distance error and improve the geolocation performance. The processor also applies Equal Gain Combining (EGC) to average out local spatial variations within a UAV. EGC is adopted due to its simplicity and fast computation. Additionally, each UAV works independently and knows its own position either by a GPS receiver or pre-planned paths. Also, it is capable of communicating with a fusion center, which makes a final geolocation decision based on the information given by multiple UAVs.

Assume an emitter is sending out RF signal and a UAV d distance away from it detected the signal at this moment. The signal propagating between these two points with no attenuation or reflection follows the free-space propagation law [10]. This commonly adopted path loss model as a function of distance is expressed as

$$\frac{P(d)}{P(d_0)} = \gamma(\frac{d}{d_0})^{-\beta} \tag{1}$$

where d_0 is a close-in distance used as a known received power reference point; β is the path-loss exponent depending on the propagation environment. γ is a unitless constant that depends on the antenna characteristics and the average channel attenuation, which can be defined as

$$\gamma dB = 20\ lg\frac{C}{4\pi f d_0} \qquad (lg = log_{10}) \tag{2}$$

where C is the speed of light and f denotes the frequency. This definition is supported by empirical data for free-space path loss at a transmission distance of 100m [11]. Based on this free-space model, the power in dB form is linearly decreasing with the increase of $log(d)$.

However, in practice, the reflecting surfaces and scattering objects will typically contribute to the random variation of RF signal transmission. The most common model for this additional attenuation is log-normal shadowing, which has been empirically confirmed to model accurately the variation in received power in both outdoor [12] and indoor [13] environments. In this case, the difference between the value predicted by the path loss model and the actual power is a log-normal random variable, i.e., normally distributed in dB, which is denoted by

$$[\frac{P(d)}{P(d_0)}]_{dB} = [\frac{\hat{P}(d)}{P(d_0)}]_{dB} + X \tag{3}$$

where X is a Gaussian random variable, with mean m and variance σ^2.

We will use the combined path loss and log-normal shadowing model to estimate the distance between RF emitter and a UAV through RSSI. The power in dB is given by

$$[\frac{P_{ri}}{P(d_0)}]_{dB} = 10lg\gamma - 10\beta lg(\frac{\hat{d}_i}{d_0}) + X \tag{4}$$

where P_{ri} is the RSSI of ES sensor i. Based on (4), when P_{ri} is detected, the processor can easily compute $\hat{d}_i$ in a dB form, which is

$$\hat{d}_{idB} = \frac{1}{\beta}\{\gamma_{dB} + \beta d_{0dB} - [\frac{P_{ri}}{P(d_0)}]_{dB}\} + \frac{X}{\beta} \tag{5}$$

Notice that $d_{idB} = \frac{1}{\beta}\{\gamma_{dB} + \beta d_{0dB} - [\frac{P_{ri}}{P(d_0)}]_{dB}\}$, therefore

$$\hat{d}_{idB} - d_{idB} = \frac{X}{\beta} \tag{6}$$

Then it is obvious that the expectation of distance mean square error based on sensor i is

$$E\{(\hat{d}_{idB} - d_{idB})^2\} = \frac{m^2 + \sigma^2}{\beta^2} \tag{7}$$

N sensors equipped on a UAV are applied to compute the local mean distance that average the local spatial variations. The estimated local mean distance is

$$\hat{D} = \frac{1}{N}\sum_{i=1}^{N}\hat{d}_{idB} \tag{8}$$

This value is obtained based on dB measurement due to the smaller estimation error compared to the linear form [14].

Notice that $D = d_{dB}$. At the detection moment, UAV is d distance away from the RF target, i.e., $d_{idB} = d_{dB}$. Also, each sensor independently obtains the $\hat{d}_{idB}$, i.e., $\hat{d}_{idB} - d_{idB}$ can be considered independent for different i, thus the expectation of *distance mean square error* for each UAV can be expressed as

$$E\{(\hat{D} - D)^2\} = \frac{m^2 + \sigma^2}{N\beta^2} \tag{9}$$

This shows that based on path loss and log-normal model, the larger number of sensor N, the smaller distance mean square error will be achieved for each UAV.

As each UAV geolocates RF emitter only based on RSSI and there is no any information about phase, in this situation the current detected area at the moment can be denoted by $a = \pi d^2$. If a is denoted by dB form, then $A = 10lg\pi + 2D$, therefore the expectation of *area mean square error* for each UAV is

$$P_A = E\{(A - \hat{A})^2\} = 4E\{(D - \hat{D})^2\} = \frac{4(m^2 + \sigma^2)}{N\beta^2} \tag{10}$$

Finally the upper bound of *geolocation area mean square error* of a UAV network can be denoted by

$$P_e = P(\bigcup_{i=1}^{R} A_i) \leq \sum_{i=1}^{R} P_{Ai} = \frac{4R(m^2+\sigma^2)}{N\beta^2} \quad (11)$$

We show this upper bound in Fig. 1, where $R = 3, m = 0, \beta = 2$ are used for illustration.

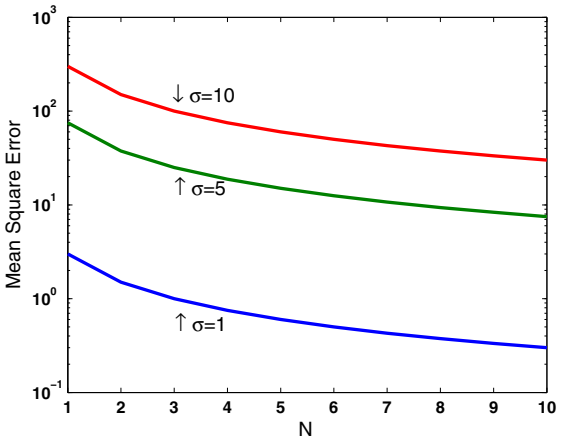

Fig. 1. Upper bound of geolocation area mean square error for a UAV network.

Apart from geolocation performance, we also define *distance range probability* as the probability that the estimated local mean distance $\hat{D}$ falls within $D_1 \leq \hat{D} \leq D_2$, where $D_1 < D_2$ and D_1, D_2 are also in dB form. The corresponding linear form of $\hat{D}, D_1$ and D_2 are $\hat{d}, d_1$ and d_2 respectively.

In order to simplify the expression, we would like to denote

$$S_i = \frac{1}{\sigma}\{\gamma_{dB} + [\frac{P(d_0)}{P_r}]_{dB} - \beta D_i + \beta d_{0dB}\}, \quad i = 1, 2 \quad (12)$$

It's obvious that $S_2 < S_1$. Therefore the distance range probability $P(D_1 \leq \hat{D} \leq D_2)$ (for simplicity, denoted by $P(D_1, D_2)$) turns out to be

$$\begin{cases} Q(S_2) - Q(-S_1) & \text{if (a)} S_1 \leq 0 \text{ or (b)} 0 < S_1 < -S_2 \\ Q(-S_1) - Q(S_2) & \text{if (c)} 0 \leq -S_2 < S_1 \text{ or (d) } S_2 > 0 \end{cases} \quad (13)$$

where the Q-function is defined as the probability that a Gaussian random Z is greater than x:

$$Q(x) = p(Z > x) = \int_x^{\infty} \frac{1}{\sqrt{2\pi}} e^{-\frac{y^2}{2}} dy \quad (14)$$

The (a)-(d) situations are illustrated in the Fig. 2. It's worth mentioning that $P(D_1, D_2) = P(d_1, d_2)$. When D_1 and D_2 are set to be values pretty close to D, (13) turns out to be the probability of correct distance range.

Based on our previous analysis, it's obvious that

$$\hat{D} = D + \frac{X}{\beta} \quad (15)$$

When the relative motion between UAV and the emitter is very slow, the mean of $\frac{X}{\beta}$, i.e., $l = \frac{m}{\beta}$ can be considered zero

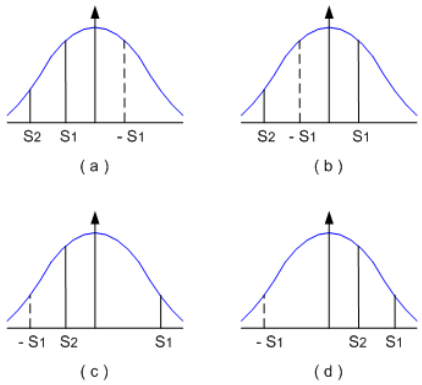

Fig. 2. Distance range probability illustration based on Q function: (a)$S_1 \leq 0$ (b)$0 < S_1 < -S_2$ (c)$0 \leq -S_2 < S_1$ (d) $S_2 > 0$.

because the mean may be considered to describe the average discrepancies in real and estimated distance between the RF emitter and the UAV during the moment of computation. Also, for simplicity and clarity, we use η to denote the variance of $\frac{X}{\beta}$, which is $\frac{\sigma^2}{\beta}$. Therefore, the probability of estimation that RF emitter locate in the range $[D_1, D_2]$ by a single UAV becomes

$$\begin{aligned} & P_{cs}(D_1, D_2) \quad (16) \\ = & \int_{D_1}^{D_2} P(D_1, D_2) f_N(u) du \\ = & \int_{D_1}^{D_2} P(D_1, D_2) \frac{1}{\sqrt{2\pi}\eta} e^{\frac{-(u-D)^2}{2\eta^2}} d\hat{D} \\ = & P(D_1, D_2)[Q(\frac{D_1 - D}{\eta}) - Q(\frac{D_2 - D}{\eta})] \end{aligned}$$

When the relative motion between the UAV and the RF emitter is obvious, due to the random variation, even the mean can be considered as a variable which follows uniform distribution in the range $[L_1, L_2]$(in dB form), where $L_1 < D_1 - D$ and $L_2 > D_2 - D$. In this case, the probability of RF emitter locating in the range $[D_1, D_2]$ by a single UAV becomes

$$\begin{aligned} & P_{cm}(D_1, D_2) \quad (17) \\ = & \int_{D_1}^{D_2} P(D_1, D_2) \int_{L_1}^{L_2} \frac{1}{\sqrt{2\pi}\eta} e^{\frac{-(u-D-v)^2}{2\eta^2}} \cdot \frac{1}{L_2 - L_1} dv du \\ = & \frac{P(D_1, D_2)}{L_2 - L_1} [\int_{L_1}^{L_2} Q(\frac{D_1 - D - v}{\eta}) - \int_{l_1}^{l_2} Q(\frac{D_2 - D - v}{\eta})] dv \end{aligned}$$

III. Netcentric Decision

As soon as each UAV obtains its distance from the RF emitter, this data will be immediately sent to a fusion center through TDMA data links. The fusion center can be a ground station or even mounted on one of the UAVs. Due to the shadowing and multiparth, the signal sent by a UAV will encounter fading before arriving at the fusion center. Assume the instantaneous signal-to-noise ratio (SNR) is y, the statistical averaging probability of error over the fading distribution [15] is

$$P_{e\_m\_f} = \int_0^{\infty} P_m(y) p_f(y) dy \quad (18)$$

where $P_m(y)$ is the probability of symbol error in AWGN based on a certain modulation scheme and $p_f(y)$ denotes the PDF of the fading amplitude.

Apply the moment generating function (MGF) $M_f(s) = \int_0^\infty p_f(y)e^{sy}dy$ and alternate Q-function $Q(x) = \frac{1}{\pi}\int_0^{\pi/2} e^{\frac{-x^2}{2\sin^2\varphi}}d\varphi$, we derive the probability of symbol error for the UAV network using 4 most common modulation schemes: phase-shift keying (MPSK), pulse amplitude modulation (MPAM), quadrature amplitude modulation (MQAM) and noncoherent frequent-shit keying (MFSK) respectively as follows:

$$P_{e\_MPSK\_f} = \frac{1}{\pi}\int_0^{\frac{(M-1)\pi}{M}} M_f(-\frac{\sin^2(\pi/M)}{\sin^2\varphi})d\varphi \quad (19)$$

$$P_{e\_MPAM\_f} = \frac{2(M-1)}{\pi M}\int_0^{\frac{\pi}{2}} M_f(\frac{-3}{\sin^2\varphi(M^2-1)})d\varphi \quad (20)$$

$$\begin{aligned} & P_{e\_MQAM\_f} \quad (21)\\ = \; & \frac{4}{\pi}(\frac{\sqrt{M}-1}{\sqrt{M}})\int_0^{\frac{\pi}{2}} M_f(-\frac{3}{2(M-1)\sin^2\varphi})d\varphi \\ & -\frac{4}{\pi}(\frac{\sqrt{M}-1}{\sqrt{M}})^2\int_0^{\frac{\pi}{4}} M_f(-\frac{3}{2(M-1)\sin^2\varphi})d\varphi \end{aligned}$$

$$P_{e\_MFSK\_f} = \sum_{n=1}^{M-1}(^{M-1}_{n})\frac{1}{n+1}M_f(-\frac{n}{n+1}) \quad (22)$$

Assume Rician fading with factor K. Two extreme cases are taken into account. If $K \to 0$, it becomes Rayleigh distribution, therefore (19)-(22) can be denoted using following expressions in this case:

$$P_{e\_MPSK\_Ray} = 1 - \sqrt{\frac{y\sin^2(\frac{\pi}{M})}{1+y\sin^2(\frac{\pi}{M})}} \quad (23)$$

$$P_{e\_MPAM\_Ray} = \frac{M-1}{M}\cdot(1-\sqrt{\frac{\frac{3y}{M^2-1}}{1+\frac{3y}{M^2-1}}}) \quad (24)$$

$$\begin{aligned} & P_{e\_MQAM\_Ray} \quad (25)\\ = \; & \frac{2(\sqrt{M}-1)}{\sqrt{M}}(1-\sqrt{\frac{\frac{3y}{2(M-1)}}{1+\frac{3y}{2(M-1)}}}) - 4(\frac{\sqrt{M}-1}{\sqrt{M}})^2 \\ & \cdot[\frac{1}{4}-\frac{1}{\pi}\sqrt{\frac{\frac{3y}{2(M-1)}}{1+\frac{3y}{2(M-1)}}}arctg\sqrt{\frac{1+\frac{3y}{2(M-1)}}{\frac{3y}{2(M-1)}}}] \end{aligned}$$

$$P_{e\_MFSK\_Ray} = \sum_{n=1}^{M-1}(-1)^{n+1}(^{M-1}_{n})\frac{1}{n+1}(1+\frac{n}{n+1}y)^{-1} \quad (26)$$

When $K \to \infty$, the Rician fading channel becomes AWGN channel. In this situation, the probability of symbol error based on above modulation schemes have been well studied and the result is provided in [10], Table 6.1.

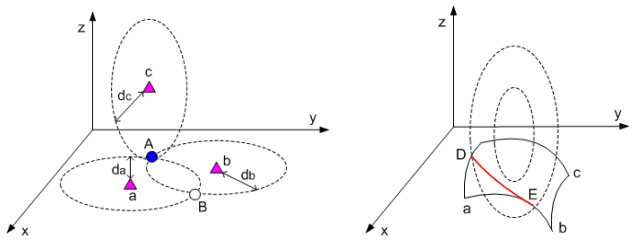

Fig. 3. RF emitter Geolocation by SUAS (a) Relative movement between RF emitter and UAVs are slow (b) Relative movement between RF emitter and mini UAVs are obvious.

According to these performance, the best modulation scheme can be chosen to reduce the probability of error. This will be further illustrated in Section IV by simulations.

For simplicity and clarity, we assume the RF emitter is on the ground surface. In the case that the relative motion between the RF emitter and UAVs are quite slow, the UAV a is able to be aware that the RF emitter is somewhere on a circle, of which the center is itself and the radius is d_a, as illustrated in Fig. 3(a). Another UAV b can also identify that there is a RF emitter on a circumference with radius d_b. After combining the information from both a and b, the fusion center will be aware that the target either locates at the position A or B. With the help of a third UAV c, the fusion center will have the knowledge that the RF emitter is at the position A. Therefore with the triangulation, 3 UAVs are able to locate the RF emitter on the ground. In the case that the target is above the ground, 4 UAVs are necessary with one more member providing altitude geolocation information.

When the relative movement between the target and UAVs are obvious, a and b will aware that the RF emitter is moving within a ring area, and the fusion system will understand that the the target is within the intersection of 2 rings. Suppose the intersection area is $\widehat{abc}$ (the intersection can also be 2 independent areas, here we use one case for illustration without loss of generality), shown in Fig. 3(b). When the data from c is obtained, its detected range ring will intersect with $\widehat{abc}$ in a line $\overline{DE}$. Therefore, the trace of the RF emitter DE will be successfully obtained. After a few numbers of measurement, the motion speed, acceleration of the target can be calculated based on range and time difference.

Due to the independence of the distance estimation by each UAV and the transmission of data to the fusion center, the probability that a single UAV accurately provides the location information to the fusion center is $P_{cs}(D_1, D_2)\cdot(1-P_{e\_MPSK\_f})$ or $P_{cm}(d_1, d_2)\cdot(1-P_{e\_MPSK\_f})$ for different relative motion situations. Thus the probability of error for the netcentric SUAS made up of R UAVs can be denoted as

$$P_{es\_Modulation} \le 1-[P_{cs}(D_1, D_2)\cdot(1-P_{e\_Modulation\_f})]^R \quad (27)$$

$$P_{em\_Modulation} \le 1-[P_{cm}(d_1, d_2)\cdot(1-P_{e\_Modulation\_f})]^R \quad (28)$$

where $Modulation$ stands for the modulation scheme. The above expressions are error upper bound, this is because the netcentric decision provides much more resilience than a single UAV. For example, in Fig. 3(a) assume UAV a and b accurately geolocate the target while c has a large location error and believes the target is far away from the pint A and B, the whole system may still provide accurate estimation if c determines that the target is closer to A compared with B. Demanding every UAV to provide accurate information to fusion center is a stringent rule, therefore (27) and (28) are upper bounds.

IV. Simulation Results and Performance Analysis

Simulations on a basis of mathematical expressions in Section II and III are presented in this Section for better analysis and illustration about SUAS performance. In the simulation, we assume $d = 100m$, $d_0 = 0.1d$, $\beta = 2$ and $R = 3$.

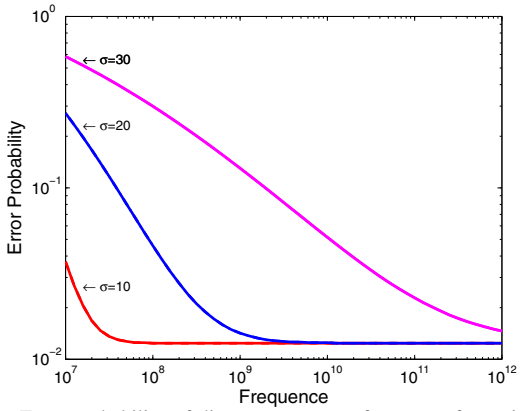

Fig. 4. Error probability of distance range vs. frequency for a single UAV.

Fig. 4 describes about error probability of distance range vs. frequency for a single UAV, where $d_1 = 0.99d$ and $d_2 = 1.01d$ have been used. The curves show that given the same σ (see (3)), the error probability of distance range will be reduced as the frequency increases. However, when the frequency is higher than a certain threshold value, such as 10^8 for $\sigma = 10$, the error probability becomes a constant. This phenomenon is the result of nonlinearity of the Q function. Therefore, this UAV system is more appropriate for geolocate an emitter with higher frequency.

Fig. 5 shows the contribution of another important factor power-rate-to-noise ratio (PRNR) to the correct probability of distance range for a single UAV. We define PRNR as $\frac{P(d_0)}{\sigma P_r}$. It is easy to observe that similar to Fig. 4, there is also a threshold value in correct probability of distance range. The larger the η (see (15)), the smaller the threshold value as well as the probability correctness.

Fig. 6-9 illustrate upper bound error probability for netcentric UAVs based on (27) and (28). Fig. 6 and 7 are in the environment of AWGN while Fig. 8 and 9 are for Rayleigh fading. In the case that relative motion between the RF emitter and UAVs are slow, $d_1 = 0.99d$, $d_2 = 1.01d$ and $\eta = 1$;

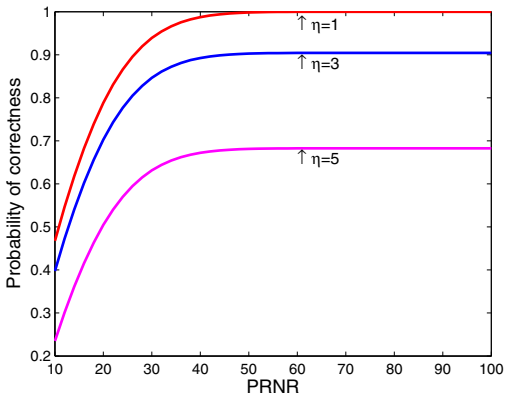

Fig. 5. Correct probability of distance range vs. power-rate-to-noise ratio (PRNR) for a single UAV.

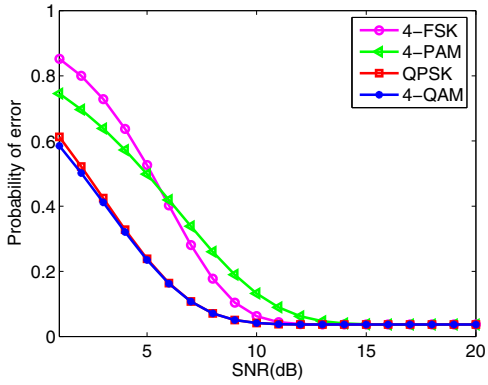

Fig. 6. Upper error bound of the netcentric UAVs in AWGN when relative movement between the RF emitter and UAVs are slow.

when the relative motion is obvious we apply $l_1 = -0.1d$, $l_2 = 0.1d$ and $\eta = 1$, therefore $P_{cs}(D_1, D_2) = 0.9876$ and $P_{cm}(D_1, D_2) = 0.94$. In Figs. 6 and 8, modulation schemes MFSK, MPAM, MPSK and MQAM with $M = 4$ are applied for illustration. This does not mean $M = 2$ can not be used. Actually, the smaller M, the smaller probability of symbol error rate for the same modulation scheme. That partially contributes to the smaller probability of error in Fig. 7. Moreover, the resilience of netcentric design makes the probability of error using BFSK and BPSK much smaller compared to that of 4-FSK and QPSK. This is the same situation while comparing Fig. 9 with 8.

These figures show that no matter the wireless radio channel between UAVS and fusion center is AWGN or Rayleigh, MQAM will provide the smallest probability of error at low SNR while MPSK will provide the smallest probability of error at moderate to high SNR. Therefore MQAM and MPSK can be applied for adaptive modulation for data fusion depending on how large the SNR is at the receiver of fusion center.

V. Conclusions

In this work, we propose a passive geolocation approach to locate RF emitter using a netcentric small UAV systems

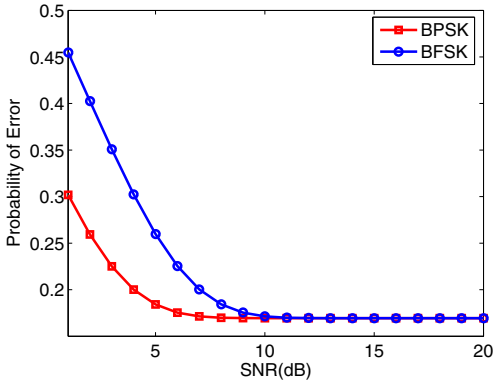

Fig. 7. Upper error bound of the netcentric UAVs in AWGN when relative movement between the RF emitter and UAVs are obvious.

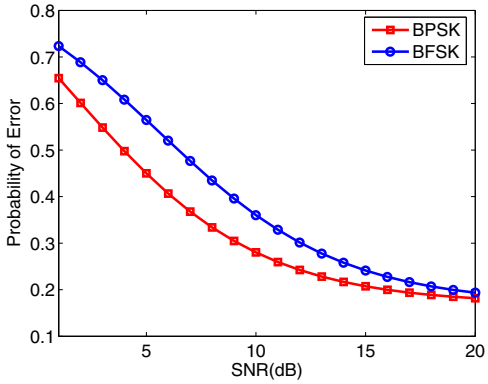

Fig. 9. Upper error bound of the netcentric UAVs in Rayleigh fading when relative movement between the RF emitter and UAVs are obvious.

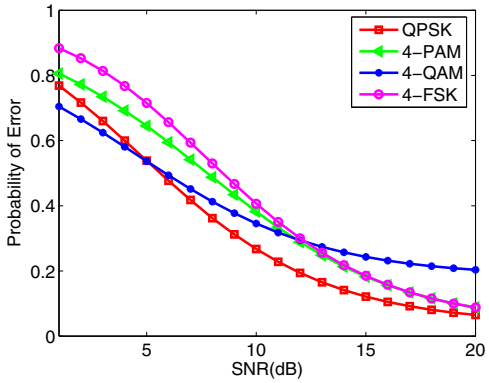

Fig. 8. Upper error bound of the netcentric UAVs in Rayleigh fading when relative movement between the RF emitter and UAVs are slow.

(SUAS) equipped with ES sensors. This approach is based on log-normal shadowing model, which has been empirically confirmed to model the variation accurately in the received power in propagation environments. We show that the geolocation error is essentially a log-normal random variable. The larger number of ES sensors, the smaller geolocation area upper bound error. We also analyze the error probability of distance range for the system. We demonstrate that when the emitter frequency is higher than a certain threshold value, the error probability becomes a constant. The situation is similar for power-rate-to-noise ratio (PRNR). Regardless what the wireless radio channel between UAVS and the fusion center is, for example AWGN, Rayleigh or Rician, at low SNR MQAM modulation is applied, while MPSK will be chosen at moderate to high SNR due to the smallest performance error of the whole system.

ACKNOWLEDGEMENT

This work was supported in part by the National Science Foundation under Grants CNS-0964713, CCF-0956438, CNS-1050618, CNS-0831902, CNS-0721515, and Office of Naval Research (ONR) under Grant N00014-07-1-0395 and N00014-07-1-1024.

REFERENCES

[1] K. C. Overman, K. A. Leahy, T. W. Lawrence and R. J. Fritsch, "The future of surface surveillance - revolutionizing the view of the battlefield", *IEEE International Radar Conf.*, pp.1-6, May 2000.

[2] D. Ledger, "Electronic warfare capabilities of mini UAVs", http://aerosonde.com.au/downloads/electronic_warfare_ledger.doc

[3] R. Madison, P. DeBitetto, A. R. Olean and M. Peebles, "Target Geolocation from a Small Unmanned Aircraft System", *2008 IEEE Aerospace Conference*, pp. 1-19, March 2008.

[4] M. Wheeler, B. Schrick, W. Whitacre, M. Campbell, R. Rysdyk and R. Wise, "Cooperative Tracking of Moving Targets by a Team of Autonomous UAVs", *2006 IEEE/AIAA 25th Digital Avionics Systems Conference*, pp. 1-9, Oct. 2006.

[5] N. Okello, "Emitter Geolocation with Multiple UAVs", *2006 9th International Conference on Information Fusion*, pp. 1-8, July, 2006.

[6] N. Okello and D. Musicki, "Measurement Association for emitter geolocation with two UAVs", *2007 10th International Conference on Information Fusion*, pp. 1-8, July 2007.

[7] L. Marsh, D. Gossink, S. P. Drake and G. Calbert, "UAV Team Formation for Emitter Geolocation", *Information, Decision and Control, 2007, IDC'07*, pp. 176-181, Feb. 2007.

[8] A. Mikhalev and R. F. Ormondroyd, "comparison of hough transform and particle filter methods of emitter geolocation using fusion of TDOA Data", *4th Workshop on Positioning, Navigation and Communication 2007, WPNC'07*, pp.121-127.

[9] F. Fletcher, B. Ristic, D. Musicki, "Recursive estimation of emitter location using TDOA measurements from two UAVs", *2007 10th International Conference on Information Fusion*, pp. 1-8, July 2007.

[10] A. Goldsmith, *Wireless Communications*, Cambridge University Press, NJ 2001.

[11] V. Erceg, L. J. Greenstein, S. Y. Tjandra, S. R. Parkoff, A. Gupta, B. Kulic, A. A. Julius, and R. Bianchi, "An empirically based path loss model for wireless channels in suburban environments", *IEEE J. Sel. Areas Commun.*, pp. 1205-11, July 1999.

[12] V. Erceg, L. J. Greenstein, S. Y. Tiandra, S. R. Parkoff, A. Gupta, B. Kulic, A. A. Julius, and R. Bianchi, "An empirically based path loss model for wireless channels in suburban environments", *IEEE J. Sel. Aresas Commun.*, pp. 1205-1211, July 1999.

[13] S. S. Ghassemzadeh, L. J. Greenstein, A. Kavcic, T. Sveinsson, and V. Tarokh, "Indoor path loss model for residential and commercial buildings", *Proc. IEEE Veh. Tech, Conf.*, pp. 3115-3119, Oct. 2003.

[14] A. J. Goldsmith, L. J. Greenstein and G. J. Foschini, "Error statistics of real-time power measurements in cellular channels with multipath and shadowing", *IEEE Trans. Veh. Tech.*, pp. 439-446, August, 1994.

[15] M. K. Simon and M.-S. Alouini, *Digital Communication over Fading Channels*, 2nd, Wiley, New Jersy, 2005.